6044 *Inorg. Chem.* **2009**, *48*, 6044–6054
DOI: 10.1021/ic900416v

Inorganic Chemistry
Article

Shape Evolution of New-Phased Lepidocrocite VOOH from Single-Shelled to Double-Shelled Hollow Nanospheres on the Basis of Programmed Reaction-Temperature Strategy

Changzheng Wu, Xiaodong Zhang, Bo Ning, Jinlong Yang, and Yi Xie*

Hefei National Laboratory for Physical Sciences at Microscale, University of Science & Technology of China, Hefei, Anhui 230026, P. R. China

Received March 2, 2009

Solid templates have been long regarded as one of the most promising ways to achieve single-shelled hollow nanostructures; however, few effective methods for the construction of multishelled hollow objects from their solid template counterparts have been developed. We report here, for the first time, a novel and convenient route to synthesizing double-shelled hollow spheres from the solid templates via programming the reaction-temperature procedures. The programmed temperature strategy developed in this work then provides an essential and general access to multishelled hollow nanostructures based on the designed extension of single-shelled hollow objects, independent of their outside contours, such as tubes, hollow spheres, and cubes. Starting from the $V(OH)_2NH_2$ solid templates, we show that the relationship between the hollowing rate and the reaction temperature obey the Van't Hoff rule and Arrhenius activation-energy equation, revealing that it is the chemical reaction rather than the diffusion process that guided the whole hollowing process, despite the fact that the coupled reaction/diffusion process is involved in the hollowing process. Using the double-shelled hollow spheres as the PCM ($CaCl_2 \cdot 6H_2O$) matrix grants much better thermal-storage stability than that for the nanoparticles counterpart, revealing that the designed nanostructures can give rise to significant improvements for the energy-saving performance in future "smart house" systems.

1. Introduction

Recently, hollow nanostructures with a controlled interior void and shell layers have received great interest for their development as ideal building blocks of lightweight structural materials and for their usage in catalysis, nanoelectronics, and drug delivery as well as energy storage.[1] To date, the effective general strategy is still much lacking for high-level generation of artificial hollow structures, and only special cases can be realized in a given reaction system. For example, the general strategy leading to complex hollow structures essentially relied on a time-consuming layer-by-layer templating technique in which the target materials and sacrificial materials are alternatively grown on the template spheres.[2] In addition, the self-assembly of surfactant molecules in aqueous solution that leads to the formation of micelles and closed bilayer aggregates provides an alternative way.[3] Very recently, our group reported the synthesis of novel double-shelled hierarchical ferrihydrite hollow spheres ($Fe_{10}O_{14}(OH)_2 \cdot 4H_2O$) via a twice-gas-bubbled template route, in which generation of the final structure is accomplished by the dissociation and hydrolysis of the cyano group and nitroso group of the added sodium nitroprusside reagent.[4]

Specially, the solid template strategy has been a rational and valuable methodology for the fabrication of nanoscale hollow objects, the interest in which has arisen because it is now relatively easy to synthesize uniform spheres and to control their size, and even the resulting hollow spheres can self-assemble into 2D and 3D colloidal arrays or photonic band gap crystals. For the hollowing process from solid templates, two main mechanisms, the Ostwald ripening process and Kirkendall effect, are usually related to the solid evacuation process. The Ostwald ripening undergoes mass transport through dissolvation and regrowth to generate

*To whom correspondence should be addressed. Tel.: 86-551-3603987. Fax: 86-551-3606266. E-mail: yxie@ustc.edu.cn.

(1) (a) Yin, Y. D.; Rioux, R. M.; Erdonmez, C. K.; Hughes, S.; Somorjai, G. A.; Alivisatos, A. P. *Science* **2004**, *304*, 711. (b) Zhang, T. R.; Ge, J. P.; Hu, Y. X.; Zhang, Q.; Aloni, S.; Yin, Y. D. *Angew. Chem., Int. Ed.* **2008**, *47*, 5806. (c) Wu, C. Z.; Lei, L. Y.; Zhu, X.; Yang, J. L.; Xie, Y. *Small* **2007**, *3*, 1518. (d) Titirici, M.; Antonietti, M.; Thomas, A. *Chem. Mater.* **2006**, *18*, 3808. (e) Yang, J. H.; Sasaki, T. *Chem. Mater.* **2008**, *20*, 2049. (f) Lou, X. W.; Deng, D.; Lee, Y. J.; Archer, L. A. *Chem. Mater.* **2008**, *20*, 6562. (g) Gao, J. N.; Li, Q. S.; Zhao, H. B.; Li, L. S.; Liu, C. L.; Gong, Q. H.; Qi, L. M. *Chem. Mater.* **2008**, *20*, 6263.

(2) (a) Yang, M.; Ma, J.; Niu, Z. W.; Dong, X.; Xu, H. F.; Meng, Z. K.; Jin, Z. G.; Lu, Y. F.; Hu, Z. B.; Yang, Z. Z. *Adv. Funct. Mater.* **2005**, *15*, 1523. (b) Yang, M.; Ma, J.; Zhang, C. L.; Yang, Z. Z.; Lu, Y. F. *Angew. Chem.* **2005**, *117*, 6885. (c) *Angew. Chem., Int. Ed.* **2005**, *44*, 6727.

(3) Xu, H. L.; Wang, W. Z. *Angew. Chem., Int. Ed.* **2007**, *46*, 1489.

(4) Wu, Z. C.; Zhang, M.; Yu, K.; Zhang, S. D.; Xie, Y. *Chem.—Eur. J.* **2008**, *14*, 5346.

 Published on Web 05/26/2009

hollow structures in which a reduction of the overall surface energy of solid particles serves as the driving force.[5] For the Kirkendall effect, the hollow nanostructures form in a way that the Kirkendall voids coalesce into a single hollow core when the coupled reaction/diffusion usually continuously occurs at the crystal/solution interface.[6] According to these two commonly accepted mechanisms, although the hollow structures have been widely explored in a large variety of hollow objects from metals to semiconductors to insulators, almost all of the synthesized hollow objects were usually simply single-shelled structures. However, much less success[7] has yet been achieved in the transformation of simple hollow objects to higher levels of synthetic hollow architectures, especially for multishelled hollow nanostructures.

Herein, by programmed control of the external reaction temperatures, the transformation from single-shelled to multiple-shelled hollow spheres occurs without any adjustment of the system itself. The strategy developed from the solid template can be designed as follows: According to the putative Kirkendall effect or Ostwald ripening, the hollowing process goes through morphology evolution from solid particles to core/shell structures and finally to completely hollowed structures. For instance, the hollowing process can be inhibited by decreasing the reaction temperature when the core/shell structure has the appropriate diameter. Then, after short-time withholding, the following hollowing process will start over to form the second shell between the first shell and the core. And then the inner core will form another internal void in the core, keeping the space between the inner core and outer shells. Consequently, if the same steps are repeated multiple times, hollow structures with multiple shells are expected to be achieved. The illustration of this strategy is shown in Figure 1. Given the known shell thickness (dt) and the neighboring shell-to-shell distance (ds) (inset in Figure 1), the multiple-shell number of hollow spheres can be given according to the formula

$$n = N\left[\frac{R}{\mathrm{dt} + \mathrm{ds}}\right] \quad (1)$$

where R and N are the sphere radius and circle number, respectively.

The hollow architectures show prospective signs for thermal energy storage based on phase-changing materials (PCMs), because they can assist in capturing solar energy directly and increase human comfort by minimizing the frequency of internal air temperature swings and maintaining the temperature close to the desired range for a longer period of time. The inorganic PCMs, which are salt hydrates, bear many advantages such as a high energy storage density and a narrow operating temperature range, but their asymmetrical melting, freezing behavior, and poor thermal cycling behavior usually restrict their potential applications in energy storage and temperature calibration.[8] In particular, realization of the encapsulation of suitable PCMs in the nanoscale-pore confinement provides an intriguing way to improve the energy-saving stability due to the fact that the PCMs were restrained in a relatively closed nanospace, where PCMs would undergo heterogeneous nucleation during the reversible melting and crystallization process to keep the thermal cycling stability. However, nanopore-confinement technology has been significantly neglected in the field of salt-hydrate PCMs for the past decades, and thus the means to improve their thermal-storage performance in the nanoscale range is still in its infant stage. Here, we employ double-/single-shelled VOOH hollow spheres as the supporting matrix to improve the application performance for thermal stability during the cycling process.

2. Experimental Section

Materials. Hydrochloric acid, hydrazine ($N_2H_4 \cdot H_2O$), $CaCl_2$, commercial V_2O_5, and ethanol were all analytical grade (Shanghai Chemical Reagents Co.) and used without further purification. Ammonium metavanadate (NH_4VO_3) was purchased from Alfa Aesar.

Preparation of the $V(OH)_2NH_2$ Precursor. A total of 2 mmol of NH_4VO_3 was loaded into a jar containing 45 mL of distilled water, and the turbid solution was strongly stirred for 10 min. Then, 1 mL of 1 M HCl solution was added to the solution at one drop per minute, ensuring that the system was a transparent yellow solution. After a given amount of $N_2H_4 \cdot H_2O$ (2, 3, 5 mL etc.) was introduced into the prepared solution and strongly stirred for 30 min at room temperature, the solid precursor $V(OH)_2NH_2$ was obtained when the homogeneous solution became turbid and its color evolved from yellow to gray. Also, the TEM image of the as-obtained solid precursor shows that most of the products were uniform solid spheres with diameter ranges from 200 to 450 nm, which then could be used as templates for the construction of single-/multiple-walled VOOH hollow spheres.

Preparation of the Single-Walled VOOH Hollow Spheres. After the above $V(OH)_2NH_2$ suspension solution was sealed in the autoclave and heated at a temperature of 120 °C for 8 h, the system was then allowed to cool to room temperature. The final product was collected by centrifugation and washed with deionized water and ethanol to remove any possible ionic remnants, and it was then dried in a vacuum at 50 °C.

Preparation of the Double-Walled VOOH Hollow Spheres. After the above $V(OH)_2NH_2$ suspension solution was sealed in the autoclave, the temperatures were programmed in several steps, rather than keeping the reaction temperatures constant in the preparation of single-shelled hollow spheres. The programmed temperature procedure is as follows:

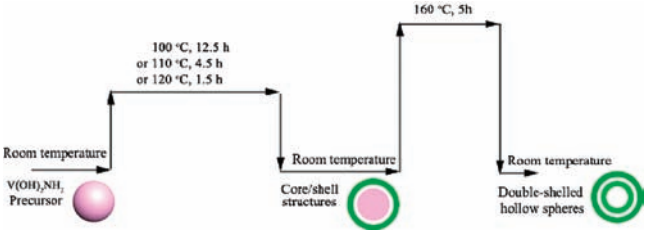

First, the sealed precursor suspension solution was heated at a temperature of 100 °C for 12.5 h, 110 °C for 4.5 h, or 120 °C for 1.5 h in order to obtain the well-defined core/shell structures that could be used for the preparation of double-shelled hollow spheres by initiating the hollowing process from the internal core. When the core/shell structures were cooled to room temperature, the whole reaction ceased, as shown in Figure 1.

(5) (a) Liu, B.; Zeng, H. C. *Small* **2005**, *1*, 566. (b) Qiao, R.; Zhang, X. L.; Qiu, R.; Kim, J. C.; Kang, Y. S. *Chem. Mater.* **2007**, *19*, 6485.

(6) (a) Fan, H. J.; Gösele, U.; Zacharias, M. *Small* **2007**, *3*, 1660. (b) Fan, H. J.; Knez, M.; Scholz, R.; Hesse, D.; Nielsch, K.; Zacharias, M.; Gösele, U. *Nano. Lett.* **2007**, *7*, 993. (c) Yin, Y. D.; Rioux, R. M.; Erdonmez, C. K.; Hughes, S.; Somorjai, G. A.; Alivisatos, A. P. *Science* **2004**, *304*, 711.

(7) Yang, J. H.; Qi, L. M.; Lu, C. H.; Ma, J. M.; Cheng, H. M. *Angew. Chem., Int. Ed.* **2005**, *44*, 598.

(8) (a) Zalba, B. E.; Je, M. M.; Cabeza, L. F. *Appl. Therm. Eng.* **2003**, *23*, 251. (b) Hawlader, M. N. A.; Uddin, M. S.; Khin, M. M. *Appl. Energy* **2003**, *74*, 195.

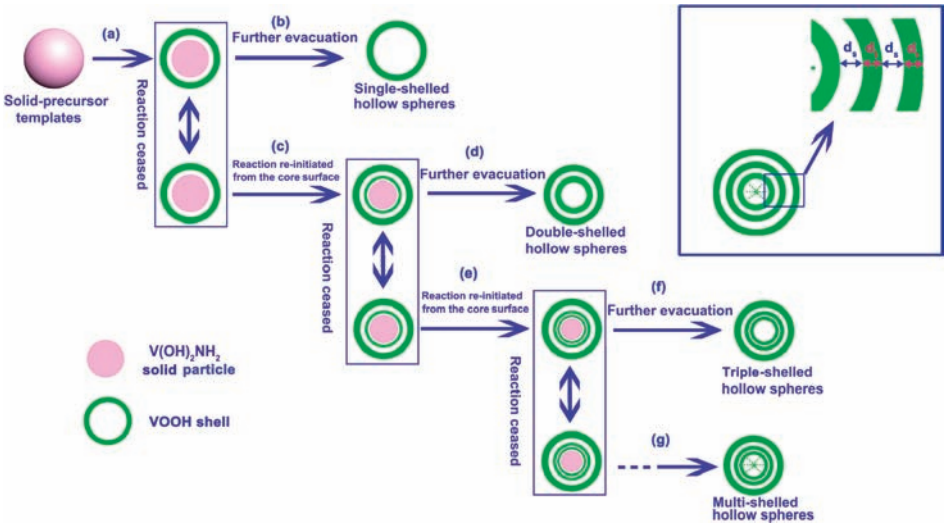

Figure 1. The schematic outline of the transformation of solid templates to single-shelled (a−b), double-shelled (a−c−d), triple-shelled (a−c−e−f), and multishelled (a−c−e−g) hollow spheres. Inset is the typical multishelled hollow spheres, where dt is the shell-thickness size and ds is the neighboring shell-to-shell distance.

In the following process, core/shell structures were further heated at the temperature of 160 °C for 5 h. The system was then allowed to cool to room temperature (20−25 °C). The double-shelled hollow spheres were collected by centrifugation and washed with deionized water and ethanol to remove any possible ionic remnants, then dried in a vacuum at 50 °C.

Characterization Method. The as-prepared sample was characterized by X-ray powder diffraction (XRD) with a Philips X'Pert Pro Super diffractometer with Cu Kα radiation (λ = 1.54178 Å). X-ray photoelectron spectroscopy (XPS) measurements were performed on a VGESCALAB MKII X-ray photoelectron spectrometer with an excitation source of Mg Kα = 1253.6 eV, and the resolution level of XPS was lower than 1 atom %. The field-emission scanning electron microscopy (FE-SEM) images were taken on a JEOL JSM-6700F SEM. The transmission electron microscopy (TEM) images were carried out on a JEOL-2010 TEM at an acceleration voltage of 200 KV. Thermal gravimetric analyses of the as-synthesized samples were carried out on a Shimadzu TA-50 thermal analyzer at a heating rate of 10 °C min^{-1} from room temperature to 600 °C.

Thermal-Energy Storage Application. The samples for VOOH−$CaCl_2 \cdot 6H_2O$ mixture systems were prepared with a mixture of 20 mg of VOOH nanoparticles and single-/double-shelled hollow spheres samples and 1.5 g of $CaCl_2 \cdot 6H_2O$ using vacuum ultrasonification for 30 min at a temperature of 35 °C. After the temperature was cooled to 0 °C, the sample was thoroughly mixed further using an agate mortar, in order to ensure that the VOOH sample was uniformly dispersed in the melting $CaCl_2 \cdot 6H_2O$. For differential scanning calorimeter measurements, samples of pure $CaCl_2 \cdot 6H_2O$ and VOOH-$CaCl_2 \cdot 6H_2O$ systems were immediately sealed in an aluminum pan for characterization by a NETZSCH DSC 200 F3 machine. For comparison, commercial V_2O_5 was also characterized using the same procedure, keeping other reaction parameters constant.

3. Results and Discussion

3.1. Preparation and Characterization of the Solid-Sphere Precursors. In our reaction systems, the solid-sphere precursors achieved by the reaction of $N_2H_4 \cdot H_2O$ and NH_4VO_3 could be collected by centrifugation of the opaque solution (see Experimental Section). The TEM image displayed in Figure 2a shows that the precursors are uniformly solid spheres with a diameter ranging from 200 to 450 nm. The XRD pattern (Figure 2b) of these as-obtained precursors shows only one broad and feeble peak in the whole range of detector angles, revealing the amorphous state of the solid-sphere precursors.

In order to further understand the chemical composition of these as-obtained solid-sphere precursors, the corresponding composition and structural characterization methods of XPS, FT-IR, and inductively coupled plasma (ICP) were applied. Important information about the surface molecular and electronic structure of the products, as well as the chemical composition, is provided by XPS, as shown in Figure 3a-1, where the spectra for elements of V, O, and N are found, with the carbon peak at 284.6 eV being a reference. The average atomic ratio of V to N is 1:1.03 on the basis of the quantification of V_{2p} and N_{1s} peaks, while the ratio of V to O is 1:2.03. Also, the value for hollow spheres (Figure 3a-1) is 515.75 eV, agreeing well with that for V^{3+}.[9] In addition, the difference in binding energy (Δ) between the O1s and V2$p_{3/2}$ level could also be used to determine the oxidation state of the vanadium oxides.[10] Here, the Δ value of the intermediate solid-sphere precursors is 14.05 eV, approaching the reported value in the literature for V^{3+}.[11] The FT-IR spectrum for the as-obtained intermediate precursor reveals that the −OH and $-NH_2$ and V−O bonds coexisted in the sample (S1).

Summarily, the combined analysis of the XPS and FT-IR results shows that the average atomic ratios of V/N and V/O are 1:1.03 and 1:2.03, respectively, and the O and N elements existing in the precursors are in the form of −OH and $-NH_2$. As a consequence, the as-obtained solid-sphere precursors can be formulated as $V(OH)_2NH_2$. Furthermore, the ICP analysis revealed the V mass content in the as-obtained intermediate precursor to be 46.9%, which matches well with the theoretical value of 49.5% for $V(OH)_2NH_2$, taking the elimination of

(9) Sawatzki, G. A.; Post, D. *Phys. Rev. B* **1979**, *20*, 1546.
(10) Mendialdua, J.; Casanova, R.; Barbaux, Y. *J. Electron Spectrosc. Relat. Phenom.* **1995**, *71*, 249.
(11) Anderson, S. L. T. *J. Chem. Soc. Faraday Trans.* **1979**, *175*, 1356.

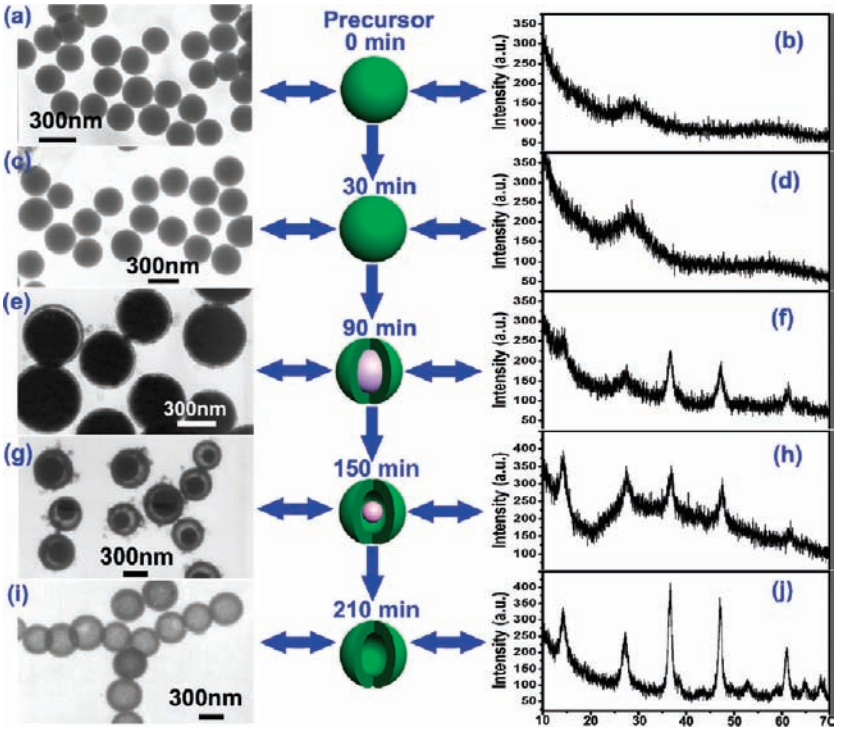

Figure 2. Schematic illustration of formation of VOOH hollow spheres. The left part shows the TEM images for the intermediate products for the morphology evolution from solid spheres (a, c), core/shell structures (e, g), and hollow spheres (i) during the formation process of single-shelled hollow spheres. The right part shows the corresponding XRD patterns for the intermediate products reacting at 120 °C after 0 min (b), 30 min (d), 90 min (f), 150 min (h), and 210 min (j).

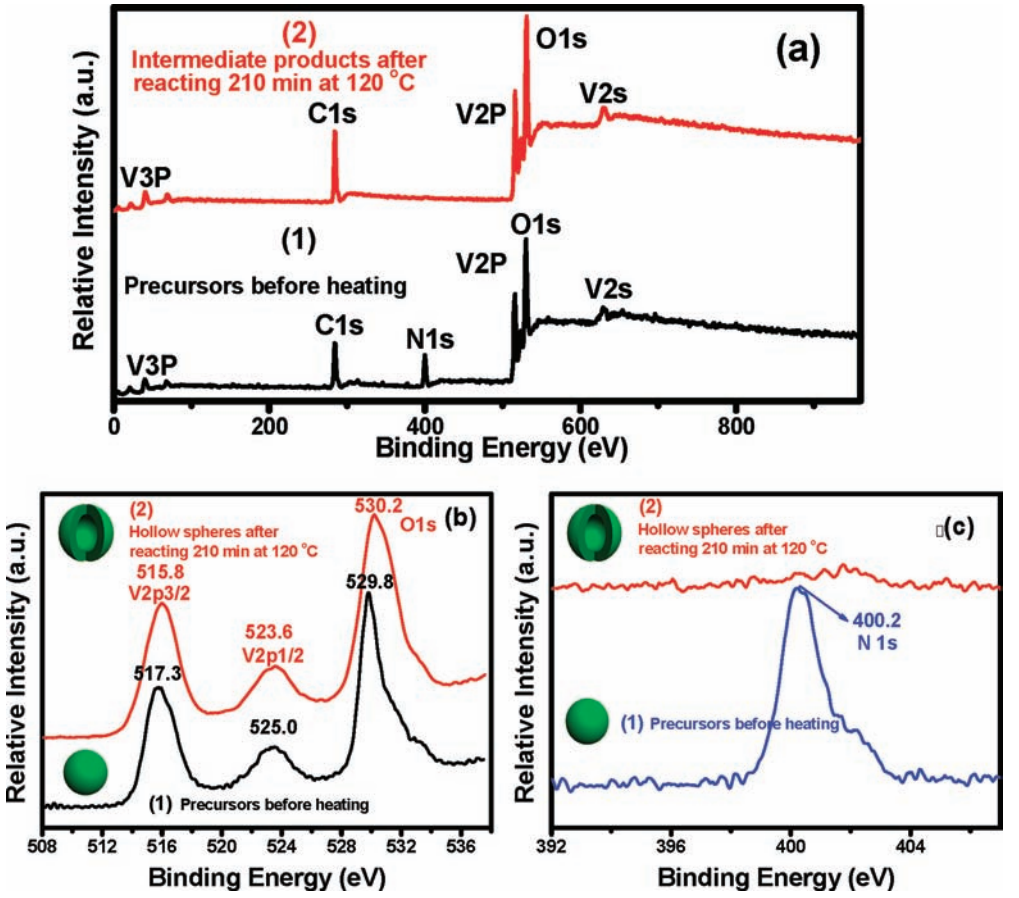

Figure 3. (a) Survey XPS spectrum, (b) high-resolution V2p region, and (c) N1s region of the $V(OH)_2NH_2$ solid-sphere precursors and the hollow spheres obtained after reacting for 210 min at 120 °C.

the H_2O absorbed on the particle surface into account. Thus, the ICP analysis verified the chemical composition of the sample to be $V(OH)_2NH_2$.

3.2. Transformation of the Solid-Precursor Templates into Single-Shelled Hollow Spheres. The time-dependent experiments at 120 °C give direct insight into the hollowing process. As shown in Figure 2, as the reaction proceeds, the diameters of the solid inner cores become smaller and smaller, with the accompaniment of increasing crystallization of VOOH, confirming the occurrence of a Kirkendall-effect-induced hollowing process. The final hollow sphere products in this reaction have been confirmed to be VOOH on the basis of the corresponding XRD pattern and the XPS characterization, which will be discussed later. The intermediate products were collected at different stages, and their morphologies and structural information were subjected to TEM and XRD investigation, respectively. In the beginning, the $V(OH)_2NH_2$ precursors have a uniform solid sphere appearance (Figure 2a), with the diameter ranging from 200 to 450 nm, and are in the amorphous state (Figure 2b). Notably, after heating at 120 °C for 30 min, the solid spheres (Figure 2c) remain as amorphous $V(OH)_2NH_2$, as confirmed by the XRD pattern (Figure 2d). However, after 90 min of heating, the thin shells start to separate from the inner core particles, and at this stage, the inner core tightly adhere to the outer shell, forming the core/shell structures (Figure 2e). Notably, the corresponding XRD pattern of the core/shell structures (Figure 2f) shows the appearance of peaks for crystalline VOOH, despite feeble intensities. As the reaction proceeds, the inner core further shrinks, making more core−shell space (Figure 2g), and the crystallization of the product further increases (Figure 2h). The inner cores are completely consumed after 210 min, resulting in well-crystallized VOOH hollow spheres (Figure 2i and j). In summary, VOOH hollow spheres were evolved through a gradual hollowing process from the amorphous $V(OH)_2NH_2$ sphere precursors, to partially crystallized core/shell structures, and finally to the well-crystallized morphology.

Moreover, through the careful analysis of XPS spectra (Figure 3) for the $V(OH)_2NH_2$ precursor and the final hollow-sphere product obtained at 120 °C after 210 min, it was evidenced that the valence of vanadium (+3) remains unchanged during the hollowing process, although the nitrogen content keeps decreasing as the hollowing process proceeds. Figure 3b shows the high-resolution XPS for the V2p and O1s region of $V(OH)_2NH_2$ precursor and the final hollow sphere product. The O1s binding energies for these two samples are almost identical (529.8 eV for the solid precursors; 530.2 eV for the hollow spheres), indicating that the oxygen atoms exist as O^{2-} species in two compounds.

The valence state of vanadium is found to be +3 for both the $V(OH)_2NH_2$ precursors and the yielded hollow spheres by looking at the $V2p_{3/2}$ core-level binding energies, which are respectively 517.3 and 515.8 eV (Figure 3b-2), in agreement with that of the bulk for V^{3+}.[9] At the same time, the difference in binding energy (Δ) between the O1s and $V2p_{3/2}$ levels could also be used to determine the oxidation state of the vanadium oxides.[10] Additionally, the Δ value for the hollow sphere product after heating at 120 °C for 210 min is 14.4 eV, which also approaches the reported value in the literature for V^{3+}.[11] Notably, there was no nitrogen in the hollow-sphere product, as shown in Figure 3c-2, although the $V(OH)_2NH_2$ precursor contains nitrogen, indicating that the reaction progress occurs from the solid-sphere precursor to the VOOH hollow sphere product.

It was suggested that VOOH hollow spheres were produced through a hollowing process based on the Kirkendall effect. It is worth noting that the $V(OH)_2NH_2$ solid-sphere precursor formed in the initial stage and H_2O can react with each other and form a diffusion pair; the coupled reaction and diffusion at the crystal−solution interface could lead to the quick formation of an interconnected VOOH nanoparticle shell around the external surfaces of the solid-sphere precursor. This process would be followed by a continuous outward flow of $V(OH)_2NH_2$ from the solution to and through the loosely packed VOOH shell to form a hollow interior and a relatively compact shell. Here, the mass transport process from the $V(OH)_2NH_2$ core particles to the immobile crystalline VOOH shells occurs coupled with the hydrolyzation reaction of $V(OH)_2NH_2$ at the $V(OH)_2NH_2$ precursor/solution interface, to form the final target material, VOOH hollow nanospheres, according to the following formula:

$$V(OH)_2NH_2 + H_2O \rightarrow VOOH + NH_4OH \quad (2)$$

3.3. Characterization of Single-Shelled Hollow Spheres. The morphology of the hollow-sphere products obtained at 120 °C for 8 h was characterized using TEM and FE-SEM images. The low-magnification FE-SEM image shown in Figure 4a indicates that the as-prepared sample is highly uniform with a high yield, and the hollow structure can be further confirmed by the higher-magnification FE-SEM image of the cracked hollow spheres, as shown in Figure 4b. As shown in the inset in Figure 4a and in part c, the hollow cavity of the as-obtained spheres is convincingly evidenced by the presence of a strong contrast between the dark edge and the pale center. Additionally, the shell boundary of the single-shelled hollow spheres is well-defined. The external diameter of the hollow spheres is 200−400 nm, and the thickness of the shell is ca. 40−60 nm.

The XRD pattern (Figure 4d) shows that the as-prepared sample is a crystallized material that corresponds to the recently discovered VOOH.[12] However, in that case, there was no available crystal structure presented. Here, the new-phased VOOH crystal cell were established by the atomic replacement and geometry optimization process, keeping the structural symmetry and atomic ratio constant, owing to the high resemblance of the atomic crystal structure of the as-obtained new-phased VOOH to that of the lepidocrocite γ-FeOOH. The constructed structure is shown in Figure 4f. The corresponding simulated XRD pattern calculated from the as-established VOOH crystal cell is almost identical to the experimental XRD pattern, supporting the established crystal structure of new-phased VOOH and thus

(12) Wu, C. Z.; Xie, Y.; Lei, L. Y.; Hu, S. Q.; Ouyang, C. Z. *Adv. Mater.* **2006**, *18*, 1727.

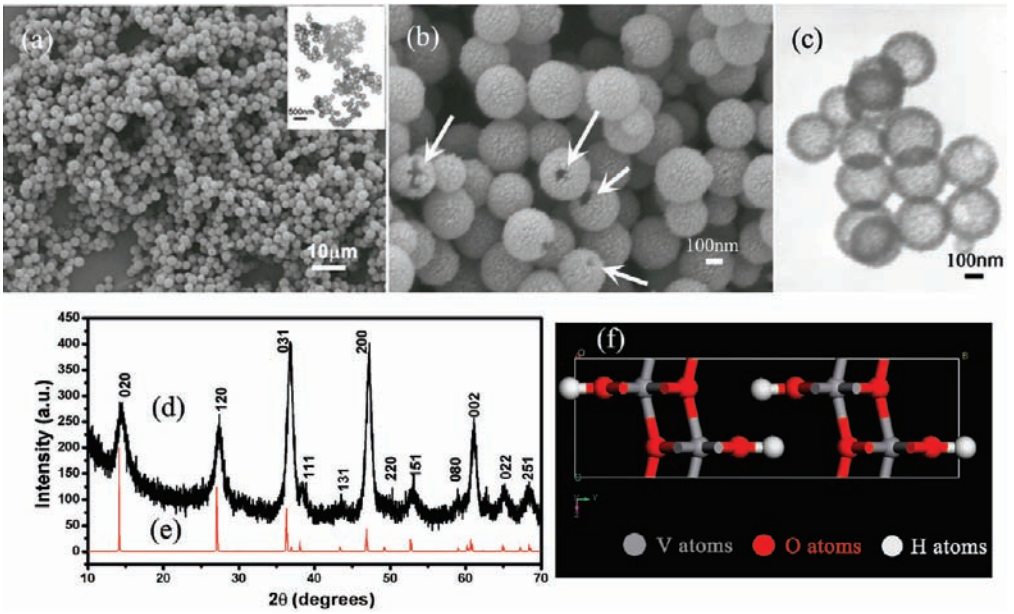

Figure 4. Low-magnification (a) and high-magnification (b) FE-SEM images and a (c) TEM image of the as-obtained VOOH hollow spheres. The inset in a shows the corresponding panoramic TEM images for VOOH hollow spheres. (d) The experimental XRD pattern for the VOOH hollow spheres. The calculated XRD pattern (e) achieved from the VOOH crystal cell (f).

providing direct evidence that it is in the lepidocrocite phase.

Moreover, the size of the hollow spheres showed strong pH dependence, which may be ascribed to the sensitivity of the $V(OH)_2NH_2$ precursor spheres to acid. Thus, by controlling the diameter of $V(OH)_2NH_2$ solid spheres via adding amounts of formic acid to adjust the pH value and partially dissolve $V(OH)_2NH_2$, we were able to manipulate the diameters of the final VOOH hollow spheres. For example, when 1 mL of formic acid (HCOOH) was added to the reaction systems, keeping the other reaction parameters unchanged, VOOH hollow spheres with an external diameter of ca. 80−150 nm were achieved, as shown in Figure 5a,b. In contrast, when 0.5 mL of formic acid (HCOOH) was added, the final hollow product usually possessed an external diameter of ca. 160−300 nm (Figure 5c,d), which is larger than that produced in the 1 mL HCOOH system but smaller than that in the no formic acid systems. All in all, the hollow-sphere diameters can be controlled to distances ranging from less than 100 to 400 nm with the addition of different amounts of formic acid.

Interestingly, the morphology of the VOOH products can also be manipulated. Also, by elevating the reaction temperature to 200 °C, the flakelike nanounits gradually grew on the surface of hollow spheres to form the "hollow-dandelion" nanoarchitectures, as shown in Figure 5e,f. The growth of nanoflakes on the surface follows the solid−solution−solid mechanism,[13] in which the VOOH nanoparticles on the surface of hollow spheres may redissolve into the solution phase and then the nanoflakes grow on the surface of spheres gradually. Here, the elevated temperature facilitates the anisotropic growth of VOOH to form a flake structure. The great anisotropy of the lepidocrocite VOOH originates from the way its crystal is packed. As shown in Figure 5g, in each layer, the VO_6 octahedra are connected with each other via edge sharing to form a 2D sheet, and the sheets are then piled into a highly anisotropic 3D crystal structure.

3.4. Reaction-Temperature Dependence of Hollowing Rates during the Kirkendall-Effect Process. Although it is usually believed that the coupled reaction/diffusion process is involved in the Kirkendall-effect process, our systematic experiments reveal that it is the chemical reaction that guided the whole hollowing process.

In our reaction systems, the hollowing rate was related to the parameters of vanadium amount and reaction time. During our hollowing process, the reaction time covers the range from the initial start point to the completely hollow state, while the molar amount of vanadium ions involved in the reaction system is 2 mmol. On the basis of systematically comparable experiments, Figure 6 shows the different morphologies at the different reaction temperatures, from which the reaction time can be clearly given from the observation of the first complete hollowing state: 990 min (100 °C), 390 min (110 °C), 210 min (120 °C), 90 min (140 °C), and 60 min (160 °C). It should be noted that it is hard to achieve a higher time-interval resolution to obtain an intermediate sample that represent the completely hollowed state under sealed hydrothermal conditions, and the data given from the setting time interval do represent the needed time data during the whole hollowing process from the solid precursors to a completely hollow state. In this case, the vanadium amount (2 mmol) divided by the reaction time gives the hollowing rate, and thus the hollowing rates at the different temperatures were given as 6.73×10^{-7} mol/L s (100 °C), 1.71×10^{-6} mol/L s (110 °C), 3.17×10^{-6} mol/L s (120 °C), 7.41×10^{-6} mol/L s (140 °C), and 1.11×10^{-5} mol/L s (160 °C). On the basis of these data, the corresponding curve diagram (Figure 6b) for the hollowing rates as a function of the reaction temperatures shows that the hollowing rate is monotonically increasing on the

(13) Sun, J. W.; Buhro, W. E. *Angew. Chem., Int. Ed.* **2008**, *47*, 3215.

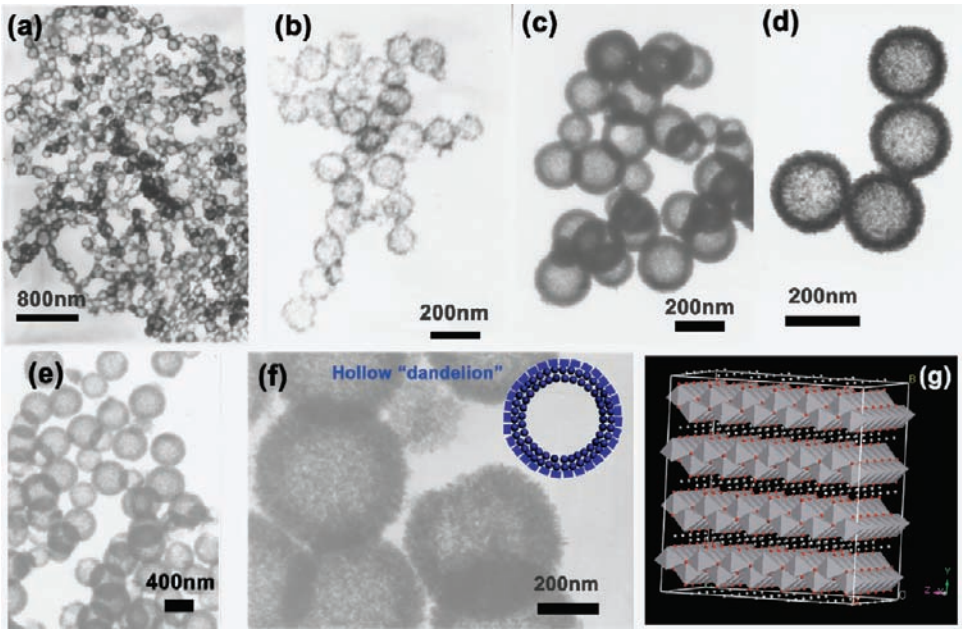

Figure 5. Controlling the diameter and outlook morphology of the hollow spheres: (a,b) TEM images of the hollow spheres with a smaller diameter size of ca. 80−150 nm by adding 1 mL of formic acid (HCOOH) to the reaction systems, keeping other reaction parameters constant. (c,d) TEM images of the hollow spheres with a smaller diameter size of ca. 160−300 nm by adding 0.5 mL of HCOOH into the reaction systems. (e,f) TEM images show the "hollow dandelion" outlook for the product obtained at 200 °C, keeping other reaction parameters constant. (g) Supercell structure for lepidocrocite VOOH.

concerned reaction temperature scale, indicating that higher temperatures significantly promote the hollowing process in our reaction systems. Also, the hollowing rates were 2−4 times higher when the reaction temperature was increased in the temperature range from 100 to 120 °C. Notably, the hollowing rate here interestingly accords with van't Hoff's rule, because for Van't Hoff's rule, a 10 °C temperature increases the reaction velocity by a factor of 2-fold or more. On the other hand, for a typical diffusion process, obviously, the diffusion coefficient was proportional to the reaction temperature (absolute temperature, T) based on the Einstein−Brown shift equation:

$$D = \frac{RT}{L}\frac{1}{6\pi\eta r} \tag{3}$$

In this formula, r is the radius of the particles, R is 8.314 J/mol/K, T is the absolute temperature, η is the viscosity of the solvent, and L is Avogadvo's number.

On the basis of eq 3, the diffusion coefficient was proportional to the reaction temperature, and it will be increased by a factor of $(T + 10)/T$ (here, T is the absolute temperature) when the 10 K temperature is elevated. That is to say, it is impossible to be 2−4 times increased at 10 K for a typical diffusion process. Therefore, the hollowing rate in our system follows the reaction velocity, rather than the diffusion rate, indicating that the chemical reaction guided the hollowing process in our Kirkendall-effect hollowing process.

Furthermore, it is well-known that, for a typical chemical reaction process, the dependence of the reaction rate (k) on the reaction temperature is given in the following formula:

$$\ln k = -\frac{\mathrm{Ea}}{RT} + B \tag{4}$$

In this formula, R is 8.314 J/mol/K, Ea is the Arrhenius activation energy, B is a constant, and T is the absolute temperature.

In our case, the diagram of ln(hollowing rate) versus a function of $1/T$ was plotted and shown in Figure 6c, where all of the experimental data points can be fit linearly with an error of −0.991, confirming the linear relationship between the experimental data points. Although it is usually believed that the coupled reaction/diffusion process is involved in hollowing process, the linear relationship further verified that it was the chemical reaction, rather than the diffusion process, that guided the Kirkendall-effect hollowing process, and the reaction rate dominated the hollowing rate.

3.5. Characterization of Double-Shelled Hollow Spheres. The double-shelled hollow spheres can be obtained by the programmed temperature procedures, in which the reaction was ceased by lowering the temperature and then initiated again by increasing the temperature, enabling the whole reaction to proceed through the designed route of (a)→ (c)→ (d), as shown in Figure 1, and form double-shelled hollow spheres. In this process, the core/shell structures with appropriate diameters of core particles should be obtained at a certain temperature first. As shown in Figure 5, in the temperature range from 100 to 160 °C, the core/shell structures with different diameters of core particles can be obtained under the appropriate reaction conditions. After the core/shell structures formed, if the following process initiated from the inner core surface to further evacuate the inner core at a relatively higher temperature (160 °C), double-shelled hollow spheres would form, keeping the void space between the inner core and outer shells.

Figure 7a,b shows the corresponding morphologies of the products obtained undergoing the temperature procedures of 120 °C for 1.5 h, room temperature for 5 h, and then 160 °C for 5 h, where the strong contrast between the

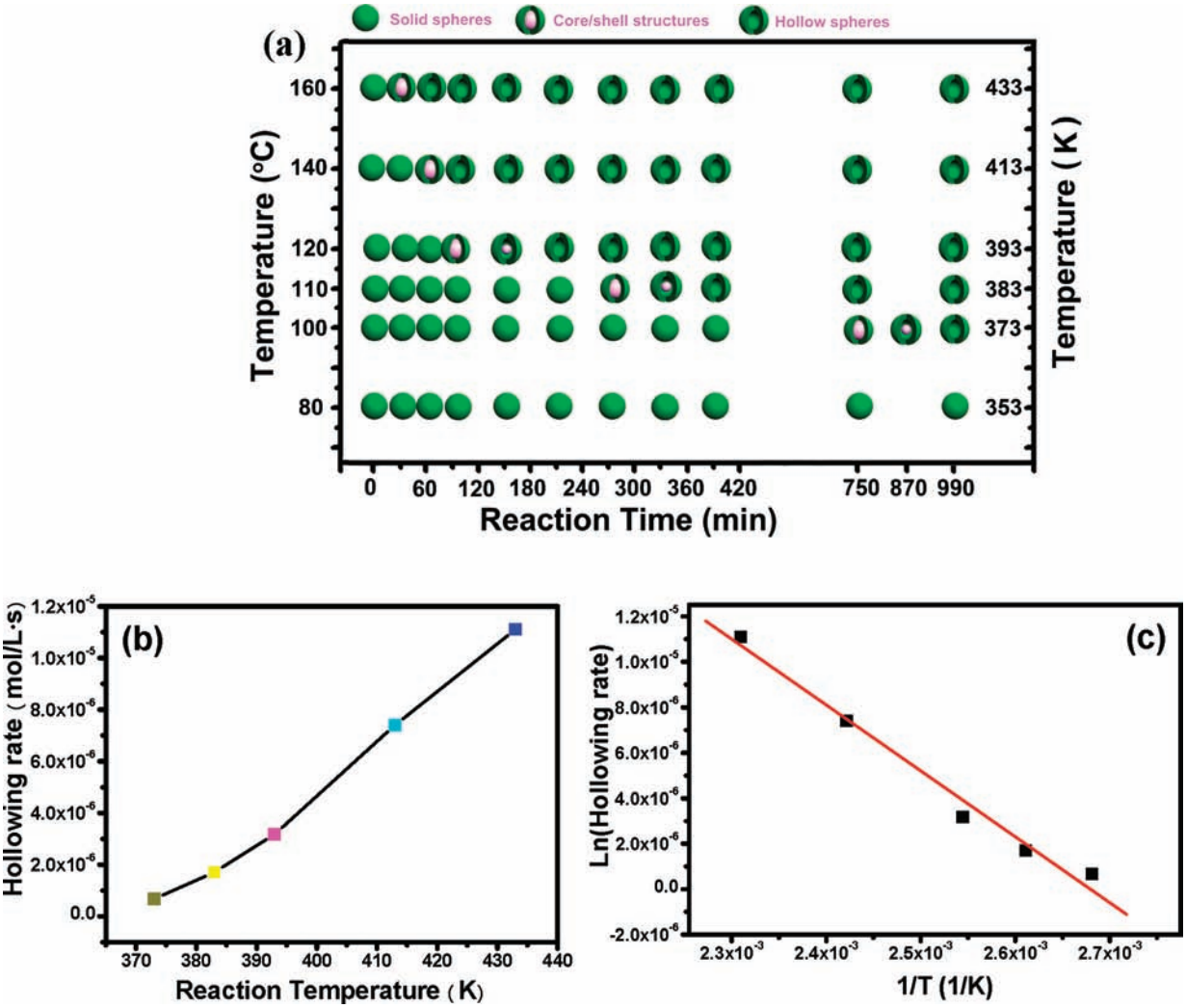

Figure 6. (a) The schematic illustration for the reaction time evolution of different morphology states at the different reaction temperatures, from which one can see that the time needed for completely hollow was significantly shortened as the reaction temperature increased. That is to say, the hollowing rates are monotonincally increasing in the concerned reaction temperature scale. (b) The curve diagram for the hollowing rate as a function of the reaction temperature. (c) The curve diagram for the Ln (reaction rate) as a function of $1/T$.

dark edge and pale center suggests a hollow cavity feature of the spherical particles. In addition, careful examination of each particle reveals that they are double-shelled hollow spheres with a small shell-to-shell distance of less than 25 nm, although the diameters of the outer contour are in the range of 300−800 nm. The wide-angle XRD pattern for these double-shelled hollow spheres, shown in Figure 7c, indicates that the as-obtained product is still orthorhombic VOOH. Furthermore, the low-magnification FE-SEM image in Figure 7d shows that all of the spherical particles are uniform with a high yield. The higher-magnification FE-SEM image (Figure 7e) of cracked hollow spheres convincingly confirmed the presence of a double-shelled shape in the as-obtained sample.

Similarly, double-shelled hollow spheres were also achieved using the other two programmed temperature procedures described in the Experimental Section, with the first step being either heating at 100 °C for 12.5 h or heating at 110 °C for 4.5 h and the other reaction parameters being the same. Figure 8a−c show the typical TEM and FE-SEM images of double-shelled hollow spheres obtained undergoing the programmed temperature procedures of 100 °C for 12.5 h, room temperature for 5 h, and 160 °C for 5 h. Their TEM images in Figure 8a,b clearly show the strong contrast between the dark solid edges and the pale hollow space, featured in the double-shelled structures. The broken spheres observed by the magnified FE-SEM image, as shown in Figure 8c, further confirm the double-shelled structure. The TEM and HRTEM images (Figure 8d−h) also show the double-shelled structure resulting from the reaction procedures of 110 °C for 4.5 h, room temperature for 5 h, and 160 °C for 5 h, revealing that the programmed-temperature route was a conventient way to prepare double-shelled hollow spheres.

It should be noted that both an appropriate core size in the core/shell structures and the reaction temperature play a crucial role in the formation of double-shelled hollow spheres. On the one hand, as for the programmed-temperature strategy, the key point lies in the initiation of the second shell from the surface of inner core particles, ensuring that the core particles evolve into other hollow spheres inside the outer spherical shells and then the double-shelled hollow spheres form. Our experimental results reveal that, if the inner core particles were not large enough, the double-shelled hollow spheres could

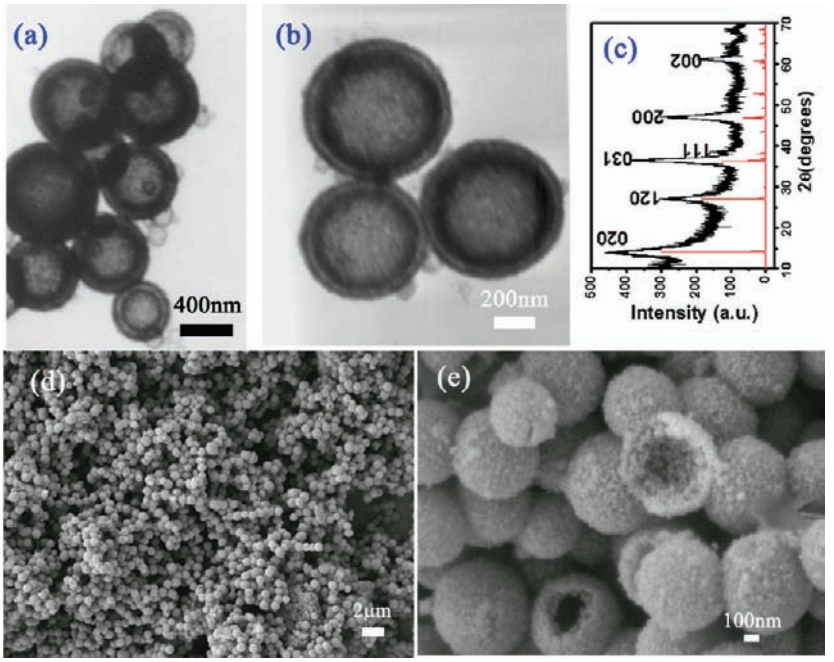

Figure 7. TEM images (a,b) and the corresponding experimental (black-color line in c) and calculated (red-color line in c) XRD patterns of the double-shelled hollow spheres obtained from the core/shell structures using temperature procedures of 120 °C for 1.5 h, room temperature for 5 h, and then 160 °C for 5 h. Low-magnification (d) and high-magnification (e) FE-SEM images of the double-shelled hollow spheres.

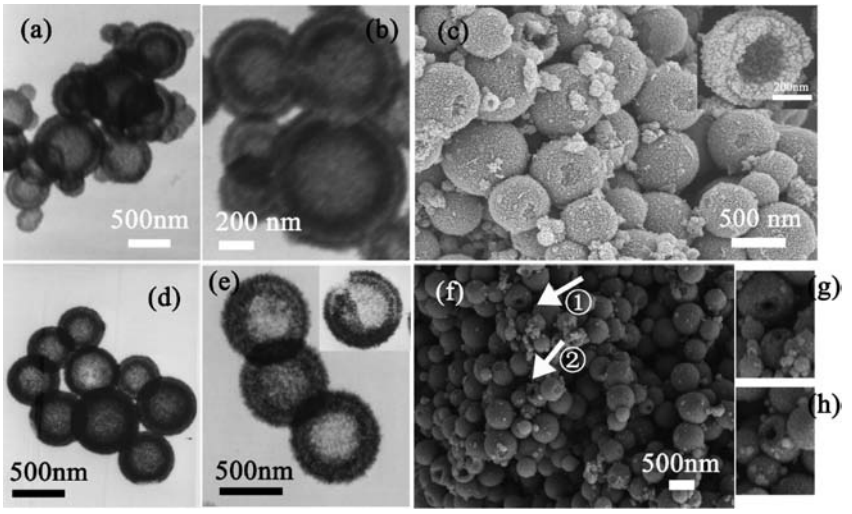

Figure 8. TEM (a,b) and FE-SEM (c) images of the double-shelled hollow spheres obtained using the programmed temperature procedures of 100 °C for 12.5 h, room temperature for 5 h, and 160 °C for 5 h, keeping other reaction parameters constant. The inset in c shows the one typical broken double-shelled hollow sphere. TEM images (d,e) and FE-SEM image (f) of the double-shelled hollow spheres obtained using the programmed temperature procedures of 110 °C for 4.5 h, room temperature for 5 h, and 160 °C for 5 h. The inset in e and parts g and h are the typical TEM image and FE-SEM images for the broken double-shelled hollow spheres.

not form, and the final product was only the single-shelled hollow spheres. For example, when the core/shell structures obtained at 120 °C for 2.5 h were introduced to the same programmed temperature-gradient procedure, due to the relatively smaller core particles, as shown in Figure 2g, only single-shelled hollow spheres were obtained. This result can be attributed to the higher surface energy possessed by smaller particles,[14] leading to continuous outward mass transport toward the outer shells and formation of the single-walled hollow spheres, rather than the double-shelled hollow spheres. On the other hand, it is apparent that the reaction temperature has a prominent effect on the formation of double-shelled hollow spheres. For instance, when the reaction temperature was higher than 120 °C, the desired core/shell structures with an appropriate core size could hardly be obtained due to hollowing rates that were too fast. Also, as for the formation of a second shell inside the first shell, the second reaction-initiated temperature (160 °C in the present work) should be higher than that for the formation of core/shell structures (usually 100, 110, and 120 °C), because the temperature difference leads to a

(14) (a) Han, Y. S.; Hadiko, G.; Fuji, M.; Takahashi, M. *Chem. Lett.* **2005**, *34*, 152. (b) Jiang, C. L.; Zhang, W. Q.; Zou, G. F.; Yu, W. C.; Qian, Y. T. *Nanotechnology* **2005**, *16*, 551.

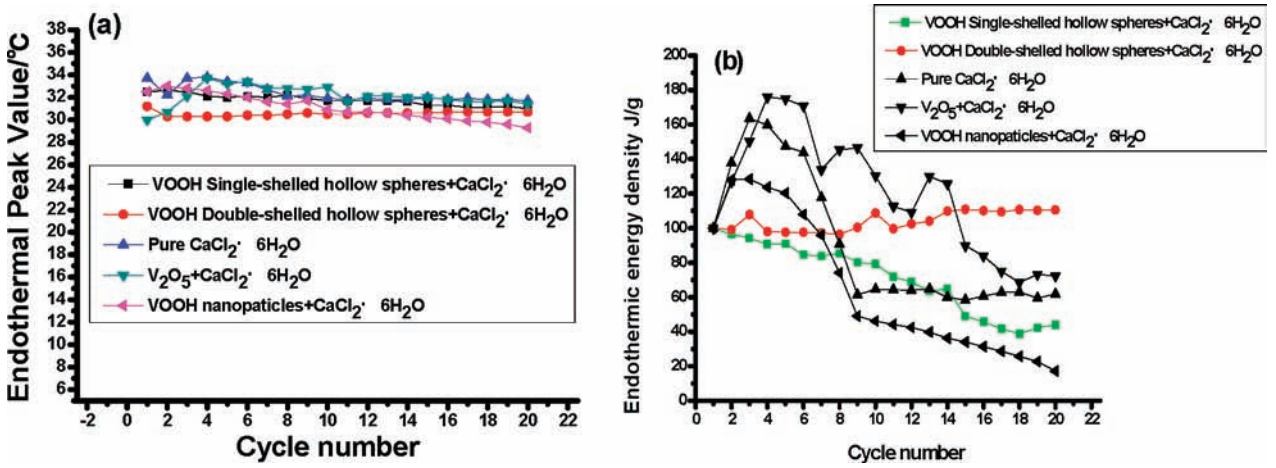

Figure 9. The cycling endothermal peak (a) and endothermic energy density behavior (b) for the single-/double-shelled hollow spheres−$CaCl_2 \cdot 6H_2O$ systems, VOOH nanoparticle−$CaCl_2 \cdot 6H_2O$ system, commercial vanadium oxides−$CaCl_2 \cdot 6H_2O$ system, and pure $CaCl_2 \cdot 6H_2O$.

discrepancy between the reaction rate and mass-transport rate that facilitates the separation of the second shell from the first shell.

3.6. Application of Single/Double-Shelled Hollow Spheres to Improve the Thermal Stability Cycling Performance. Employing the double-/single-shelled VOOH hollow spheres as a supporting matrix has advantages in terms of thermal stability during the cycling process. Herein, the testing samples were prepared by means of a vacuum-ultrasonication impregnation method, and these samples were named as follows: sample 1 (VOOH single-shelled hollow spheres + $CaCl_2 \cdot 6H_2O$), sample 2 (VOOH double-shelled hollow spheres + $CaCl_2 \cdot 6H_2O$), sample 3 (VOOH nanoparticles (S3) + $CaCl_2 \cdot 6H_2O$), sample 4 (commercial V_2O_5 + $CaCl_2 \cdot 6H_2O$), and sample 5 (pure $CaCl_2 \cdot 6H_2O$). As shown in Figure 9, although the endothermal peaks for all of the samples from sample 1 to sample 6 approached close to 30 °C, the endothermal energy density exhibited a large discrepancy for each sample. In order to precisely illustrate the data deviation for these samples, the standard deviations (σ) were calculated for each sample to evaluate how widely spread the values in the data were, on the basis of the following formula:

$$\sigma = \sqrt{\frac{1}{N}\sum_{i=1}^{N}(x_i - \bar{x})^2} \qquad (5)$$

where x_i is the data point value, $\bar{x}$ is the mean of all data point values, and N is the data point number.

According to the calculation results, sample 2 of the double-shelled hollow spheres−$CaCl_2 \cdot 6H_2O$ system has the lowest standard deviation value of 5.66. In ascending order, their standard deviation values were 20.77 (sample 1, single-shelled hollow spheres−$CaCl_2 \cdot 6H_2O$ system), 35.1 (sample 4, commercial V_2O_5−$CaCl_2 \cdot 6H_2O$), 39.09 (pure $CaCl_2 \cdot 6H_2O$), and 40.16 (sample 3, VOOH nanoparticles−$CaCl_2 \cdot 6H_2O$). That is to say, with the participation of single-/double-shelled hollow spheres as the matrix, the corresponding thermal stability possesses much better performance when compared with that of other samples. Notably, the high standard deviation for the VOOH nanoparticles−$CaCl_2 \cdot 6H_2O$ system (sample 3) reveals that simple nanoparticles without any porous confinement have no improvement in thermal stability, indicating that the nanoporous cavities in the hollow spheres play a crucial role in maintaining thermal stability during the cycling process. As for nonporous structures, such as VOOH nanoparticles, commercial vanadium oxides, and pure $CaCl_2 \cdot 6H_2O$, all of the cycling processes were carried out in relatively open systems, where the phase separation and homogeneous nucleation occur,[15] leading to relatively poor cycling stability. In particular, the excellent cycling thermal stability for the double-shell hollow spheres lies in their morphological feature in which there are two kinds of space cavity and double-layered shells, which makes it hard to escape from the sealed environments for the impregnated $CaCl_2 \cdot 6H_2O$. In the relatively confined smaller space, heterogeneous nucleation would answer for the excellent cycling performance for thermal energy storage by mitigating the phase separation problems. The single-shelled hollow spheres have only one thinner layer of nanoparticles with a hollow cavity inside. In this case, the impregnated $CaCl_2 \cdot 6H_2O$ is still likely to penetrate into the exterior space during volume expansion in the melting state of inorganic salt hydrates, leading to lesser cycling stability for $CaCl_2 \cdot 6H_2O$. In other words, employing the confined porous nanocavity in the single-/double-shelled hollow spheres as the matrix successfully achieved excellent endothermal storage stability for inorganic hydrated salts, providing a new avenue for the improvement of energy-saving performance for the salt-hydrate PCMs.

4. Conclusions

In summary, we have described a new and convenient route to synthesize double-shelled hollow spheres from solid templates only by programming the reaction-temperature procedures. Since, during the past decades, it has already been well accepted that the solid templates can only be introduced to synthesize the single-shelled hollow objects, the programmed temperature strategy developed here then provides an essential route for the designed extension of the solid templates to multishelled hollow nanostructures, not limited to the single-shelled ones, opening up new opportunities for the preparation of higher levels of artificial hollow architectures independent

(15) (a) Lu, K.; Li, Y. *Phys. Rev. Lett.* **1998**, *80*, 4474. (b) Huang, J. F.; Bartell, L. S. *J. Phys. Chem.* **1995**, *99*, 3924.

of their outside contour, such as tubes, spheres, and cubes. Furthermore, using the double-shelled hollow spheres as the PCM ($CaCl_2 \cdot 6H_2O$) matrix grants a much better advantage in thermal-storage stability when compared with that for nanoparticles, revealing that designable nanostructures can give rise to significant improvements for energy-saving performance in future "smart house" systems.

Acknowledgment. This work was financially supported by the National Basic Research Program of China (No. 2009CB939901), National Natural Science Foundation of China (No.20621061, 20801051), and China Postdoctoral Science Foundation funded project (No. 200801235, 20080430102).

Supporting Information Available: The characterization of the $V(OH)_2NH_2$ solid-sphere precursors, supplemental TEM information for Figure 5a, the preparation details and characterization of VOOH nanoparticles, and crystallographic information file for the new-phased Lepidocrocite VOOH are given. This material is available free of charge via the Internet at http://pubs.acs.org.